

Impact of Radio Frequency Plasma Power on the Structure, Crystallinity, Dislocation Density, and the Energy Band Gap of ZnO Nanostructure

Ahmed F. Abdulrahman, Azeez A. Barzinjy,* Samir M. Hamad, and Munirah Abdullah Almessiere

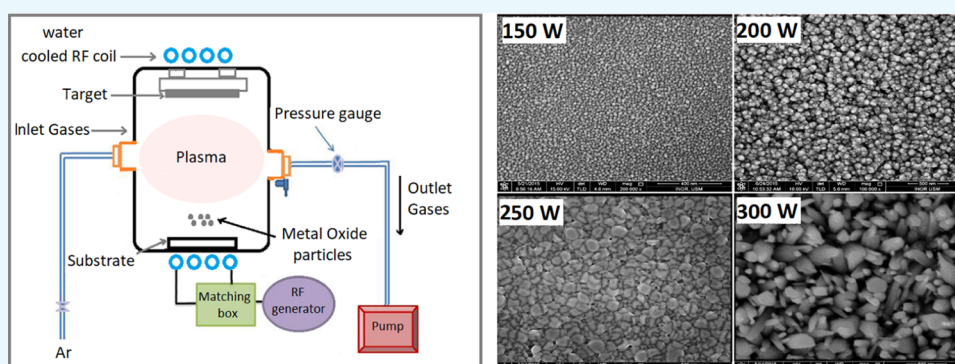
Cite This: *ACS Omega* 2021, 6, 31605–31614

Read Online

ACCESS |

Metrics & More

Article Recommendations



ABSTRACT: The aim of this study is to investigate the effect of radio frequency (RF) plasma power on the morphology, crystal structure, elemental chemical composition, and optical properties of ZnO nanostructure using a direct current magnetron sputtering technique. This study emphasized that the growth rate and surface morphology of the polycrystalline ZnO were enhanced as the radio frequency (RF) plasma power increased. This can be observed by fixing other parameters such as the growth time, substrate temperature, and chamber partial pressure. The RF plasma power alteration from 150 to 300 W can produce uniform nanograin, spheroid, and nanorods. Additionally, the RF plasma power alteration leads to the alteration in the ZnO nanorod diameter from 14 to 202 nm. It was observed that the XRD intensities are increased at higher plasma powers. This, perhaps, can be inferred from the transformation of the granular microcrystals to the needlelike or platelike large crystals, as already examined using SEM images. This also has an impact on the average crystalline size, which increased from 10 to 40 nm on increasing the RF plasma power. Moreover, the increase of the RF plasma power has an obvious impact upon the optical band-gap energy, which was accordingly decreased from 3.26 to 3.22 eV. Finally, the absorption band edge was shifted to a lower-energy region due to the quantum size effect at the nanorange.

1. INTRODUCTION

Metal oxide nanostructured materials play an important role due to their high usage in the fields of photonic and optoelectronic devices.^{1,2} Several types of metal and metal oxide materials have been produced with different structures and optical and electrical properties to achieve the necessities of preferable applications. Among them, zinc oxide (ZnO) has attracted worldwide attention due to its adaptable properties for applied-science applications.³ ZnO is an n-type semiconductor material and has a direct band gap of 3.37 eV and exciton binding energy of 60 meV at room temperature.⁴ Furthermore, it is potentially useful in various applications including UV light-emitting devices,⁵ nanosensors,⁶ energy conversion and storage,⁷ and thin films and solar cells.^{8,9} ZnO materials are mostly fabricated using conventional deposition methods, such as physical vapor deposition (PVD),¹⁰ electro-

deposition,¹¹ chemical vapor deposition (CVD),¹² pulsed laser deposition,¹³ sol-gel method,¹⁴ spray pyrolysis,¹⁵ hydrothermal method,¹⁶ and magnetron sputtering.¹⁷ Among these methods, magnetron sputtering is a flexible technique for the synthesis of ZnO materials. Extensive work has been done using RF-magnetron sputtering due to the high growth rate, low growth pressure, and low growth temperature.¹⁸ Magnetron sputtering works based on the reactor design, target materials, RF plasma source and power, distance between

Received: August 1, 2021

Accepted: November 2, 2021

Published: November 17, 2021



targets and substrate, partial pressure, and substrate temperature.¹⁹ Moreover, RF plasma sputtering has several advantages, as it does not involve high temperature and reduces the stress and strain caused by the differences in thermal expansion coefficients between the substrate and the growth structure.²⁰ In the magnetron sputtering technique, the RF power is a significant growth parameter that directly influences the morphology, crystal structure, and optical and electrical properties of ZnO films.²¹ The effect of the RF plasma power during the growth of materials is critical since the plasma power is strongly related to the kinematics of the reactive species that is mostly incorporated in growing ZnO structures such as electrons, ions, atoms, and molecules.²²

In this study, ZnO nanostructures have been synthesized using the RF-magnetron sputtering method. The effect of different plasma powers ranging from 150 to 300 W on the surface morphology, growth structure, elemental compositions, and optical properties of the ZnO nanostructures has been examined. This has been conducted to optimize the growth plasma power to obtain a high-quality ZnO nanostructure. The results demonstrated that the morphology and the crystal structural characteristics of the ZnO nanostructure can be acclimated by RF plasma power.

2. EXPERIMENTAL DETAILS

The ZnO nanostructures were grown and deposited on glass substrates utilizing the direct current radio frequency (RF) sputtering magnetron technique, using an Auto HHV 500 sputter coater model and ZnO target (99.999% purity), with a 3-in. diameter and a 0.125-in. thickness purchased from Kurt J. Lesker Inc. Company. The glass substrates were cleaned in an ultrasonic bath using ethanol (96%), acetone, and deionized water for 15 min, respectively. The ZnO nanostructures were grown using argon gas with 5.5×10^{-6} bar pressure inside the RF chamber with different RF powers for 60 min. A schematic illustration of the RF plasma power system is shown in Figure 1.

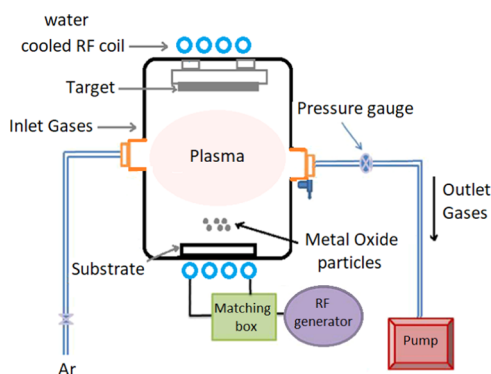


Figure 1. Diagram of the RF plasma power system.

To investigate the effect of different power values of RF on the ZnO nanostructural properties, the RF plasma power was altered from 150 to 300 W by increasing by 50 W each time gradually, and the corresponding samples were labeled a, b, c, and d, respectively. Then, the ZnO nanostructure samples were taken off from the RF system and annealed at 300 °C under a standard atmosphere, 760 mm mercury, for 30 min using an annealing tube furnace model Lenton VTF/12/60/700. A high-resolution field emission scanning electron microscope

(FESEM) (model Carl Zeiss, Leo-Supra 50 VP, Germany) and a Nova Nano SEM 450-FEI, the Netherlands, were employed to examine and characterize the surface morphology (density, shape, size, homogeneity, and distribution), and energy-dispersive X-ray (EDX) spectroscopy was used to analyze the chemical composition of the produced ZnO nanostructure. Also, a high-resolution X-ray diffraction (HR-XRD) system (model X-Pert Pro MRD) with Cu K α ($\lambda = 0.154050$ nm) radiation was used to examine and analyze the X-ray pattern and the crystal structure. The crystal quality, size, strain, stress, and epitaxial growth of the synthesized ZnO nanostructure in the scanning range of 2θ (2θ set between 20 and 80°) can be found from the XRD peaks. In addition, a double-beam ultraviolet–visible (UV-4100) spectrophotometer was utilized to analyze optical properties such as the transmittance spectrum and the band gap of the prepared ZnO nanostructure in the wavelength range of 300–800 nm.

3. RESULTS AND DISCUSSION

3.1. Morphological Analysis. To investigate the effect of plasma power on the ZnO nanostructure, several samples have been synthesized at different plasma powers. The top view and the cross-sectional growth of the ZnO samples were studied using field emission scanning electron microscopy, as shown in Figure 2. At a lower plasma power, i.e., 150 W, it was observed that the ZnO nanograins were formed with homogeneous distribution on the entire glass substrate, while at 200 W plasma power, nanospheroids were observed. Later, when the plasma power reached 250 W, agglomerated nanorods were detected. Then, at 300 W, rough surface nanorods with nonhomogeneity in shape, size, and growth direction were formed. It can be observed, from Figure 2, that the overall resulting nanostructures were almost oriented along the *c*-axis [0001] direction on the glass substrate with different plasma powers. It can be stated that on increasing the RF plasma power, the temperature also increases inside the reactor. This is, perhaps, due to the enhancement in the plasma density, i.e., the temperature of electrons or ions.²³ El-Hossary et al.²⁴ studied the impact of plasma power on ZnO thin-film deposition. They observed that an increasing RF plasma power resulted in higher plasma species energy, owing to the increase of the substrate temperature.²⁴ In the current study, we observe in all samples the alteration of ZnO morphology with different plasma powers, conceivably ascribed to the gradual temperature increase of the growth substrate. Besides, this can also be understood as an improvement of the kinetic energy of the plasma species, leading to the addition of reactive ZnO atoms.²⁵ Moreover, from the field emission scanning electron microscopy images in Figure 2, the average values of the nanostructure's diameter are highly influenced by the plasma power. One can assume from the superficial calculations, from Figure 2, that the average diameter of the formed ZnO nanostructures is gradually increased from 14 to 202 nm as the plasma power is increased from 150 to 300 W. This increase in the ZnO nanostructure's diameter with RF power is possibly due to the enhancement in the kinetics of the additional atoms and also the aggregation of the individual nanostructures, which results in a bigger size of the ZnO nanostructures at higher RF powers.²⁵ Karnati et al.²⁶ in a similar study, using the high-pressure-assisted pulsed laser deposition (PLD) technique, synthesized high-quality vertically aligned ZnO nanorods on different substrates at a high growth pressure of ~ 0.3 Torr. The rise in the substrate

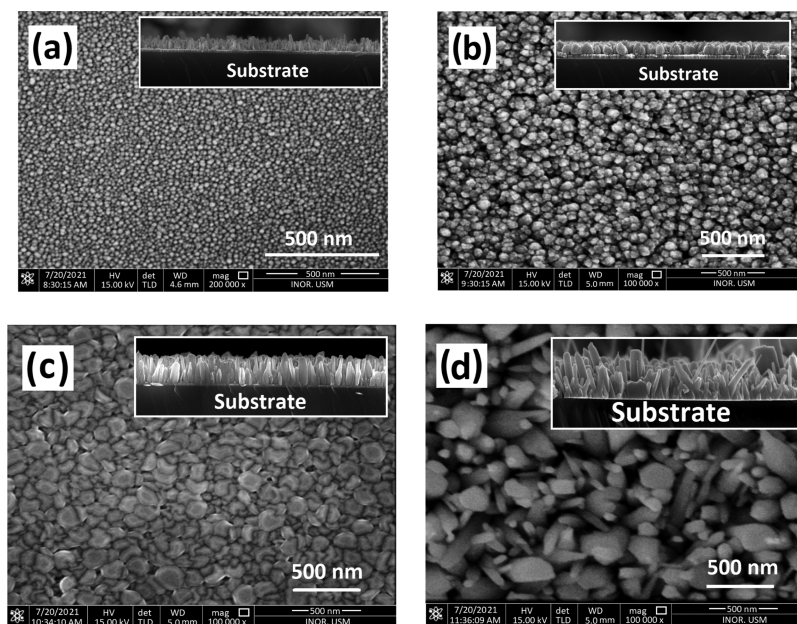


Figure 2. Top view and the cross-sectional (inset) field emission scanning electron microscopy image of the ZnO nanostructure synthesized with different RF plasma powers: (a) 150 W, (b) 200 W, (c) 250 W, and (d) 300 W.

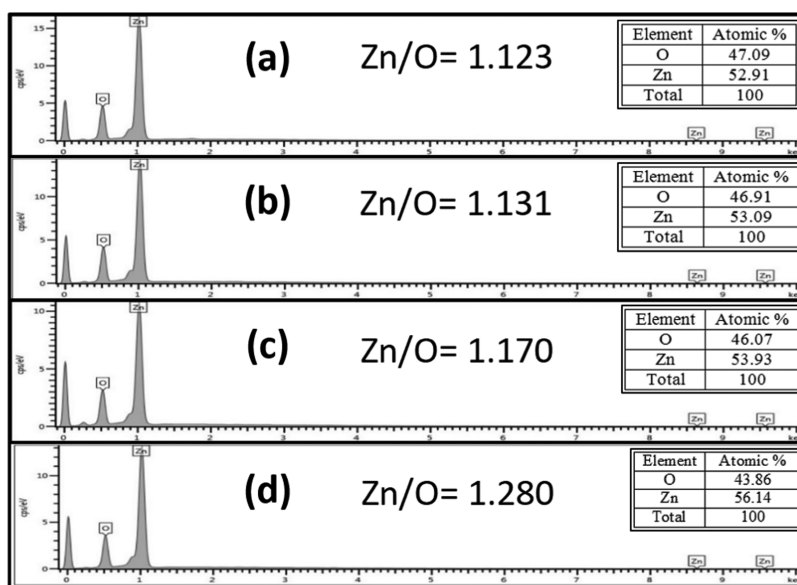


Figure 3. EDX analysis of the ZnO nanostructure synthesized with different RF plasma powers: (a) 150 W, (b) 200 W, (c) 250 W, and (d) 300 W.

temperature leads to an increase in the diameter of the nanorods, which essentially relies upon the growth mechanism and the stress between the substrate and the nanorods. They also stated that the nanorods have a tendency to bend as the number of pulsed laser shots increases, which predominantly relies upon the steadiness of the nanorods.²⁷ Accordingly, temperature and the number of pulsed laser shots throughout the deposition play vital roles in the alignment of the ZnO nanorods.

3.2. Energy-Dispersive X-ray (EDX) Analysis. To study the elemental composition of the synthesized ZnO nanostructure using the RF sputtering technique, EDX analysis has been utilized for different plasma powers from 150 to 300 W, as shown in Figure 3a–d. From Figure 3, it can be seen that the corresponding EDX analysis shows the existence of Zn and O

peaks only, which corresponds to the characteristic elemental composition of the ZnO nanostructure, without the presence of any other impurities or substrate signal. This is a good indicator for the purity of the grown ZnO nanostructures by means of RF plasma power. The estimated Zn and O percentage ratios of the synthesized samples at different plasma powers are tabulated in the insets in Figure 3a–d. An approximate stoichiometry in the Zn/O ratio can be noticed from the EDX analysis. While the atomic percentage ratio between Zn and O for the samples was slightly different, the Zn/O ratio increases with increasing plasma power (Figure 3). This is likely because, at low RF plasma power, some of the zinc atoms can be masked by the incoming species before being oxidized. These results are in excellent agreement with those of El-Hossary et al. and Otieno et al.^{24,28} Otieno et al.,²⁸

in turn, stated that an increasing stoichiometry, Zn/O ratio, leads to an increase in the strain and the dislocation density of the ZnO films. These outcomes are also consistent with the field emission scanning electron microscopy images since the RF plasma power affects the morphology of the ZnO films. Accordingly, the interface between O and Zn atoms is altered to form ZnO thin films with dissimilar stoichiometry, dissimilar crystalline sizes, and diverse morphologies.²⁴ Also, increasing the RF power leads to a decreasing band gap, owing to the existence of zinc hydroxide, Zn(OH)₂. This leads to a decrease in the oxygen content in the sample. On the other hand, it has been reported, previously by other authors, that it is not easy to deposit multicomponent materials with highly precise stoichiometry using various substances since dissimilar substances possess dissimilar vaporization rates.²⁹ It is significant to mention that an alteration of RF plasma power can change the ionization of ambient argon gases,³⁰ the kinetic energy of bombarding ions,³¹ kinetic energy of atoms,³² reactive species,³³ and the substrate temperature.³⁴ Therefore, we are likely to manage the stoichiometry of the ZnO film basically by modifying the ambient working gas in RF plasma deposition.³⁵

3.3. X-ray Diffraction (XRD) Analysis. The X-ray diffraction (XRD) patterns of the ZnO nanostructure grown on the glass substrates at different RF plasma powers are shown in Figure 4. It can be seen that the XRD patterns, in

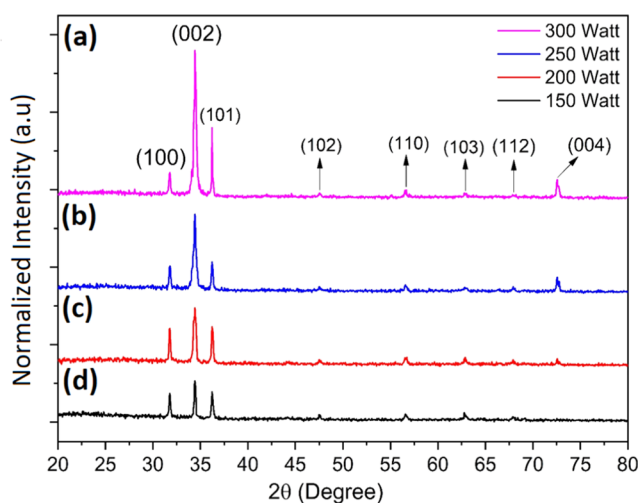


Figure 4. Normalized X-ray diffraction patterns of the ZnO nanostructure synthesized with different RF plasma powers: (a) 300 W, (b) 250 W, (c) 200 W, and (d) 150 W.

general, using different RF plasma powers possess a polycrystalline structure. In addition, the XRD diffraction analysis approves the formation of an uncontaminated hexagonal (wurtzite) structure of ZnO in accordance with JCPDS card no. 01-080-0074. Moreover, no other peaks from impurities or defects were observed. In all cases, the peak at $2\theta = 34.4$, corresponding to the (002) plane, is dominant and shows preferential growth directed along the *c*-axis as a result of having high kinetic energy.

Therefore, the (002) plane has the fastest growth rate and surface energy compared to the growth along other planes. Accordingly, this peak plays a crucial role in column growth compared to the other planes such as (101) and (100), which possess relatively lower surface energy (Figure 5). Hu et al.

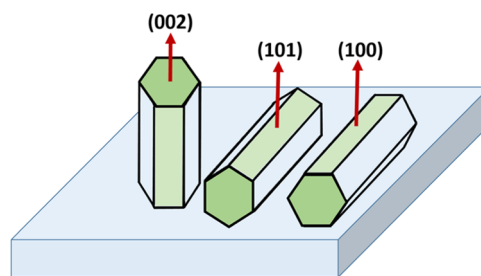


Figure 5. Crystal growth orientation of ZnO films for (002), (101), and (100) planes on the glass substrate.

reported that the (101) and (100) planes possess relatively weak intensity peaks compared with the (002) plane owing to their textured pyramid-like and polygon structures, respectively.³⁶ In general, as confirmed by X-ray diffraction, increasing the RF plasma power is found to improve the crystallinity and the grain growth, resulting in a less defected structure.³⁷ This was also confirmed by Srinatha et al.³⁸ particularly when Al-doped ZnO thin films were replaced with ZnO thin films.

Figure 5 displays the crystal growth orientations of the ZnO films. The (002) plane corresponds to the *c*-axis growth, which is perpendicular to the substrate to form a columned structure. The (101) plane corresponds to the *c*-axis growth, which is parallel to the utilized substrate forming a pyramid-like structure. The (100) plane corresponds to the *c*-axis growth, which is also parallel to the substrate to form a polygon structure. These results are mainly important as ZnO thin films can be used as front electrodes in solar cells, especially with amorphous silicon being used as a substrate.³⁹ Similar results have been found elsewhere by Jagadale et al., and they have shown that the ZnO film with these properties can be used in gas-sensing applications.⁴⁰ Bhaumik et al.⁴¹ showed that outstanding solar cell appearances, with record maximum efficiency, can be obtained with ZnO/CuO-based thin films. Moreover, the ZnO nanostructure is a suitable material owing to its photocatalytic activity for environmental and energy applications.⁴²

It can be seen from Figure 6 that the intensity of the (002) plane increases on increasing the utilized RF plasma power. From this, we can deduce that the ZnO structure is preferentially oriented in the (002) plane, which grows perpendicularly on the substrate forming a columned structure. Similar results have been obtained by El-Hossary et al.²⁴

3.4. Structural Properties. Table 1 shows properties, such as peak position (2θ), intensity, lattice constants (*a* and *c*), aspect ratio (*c/a*), and the strains (\sum_c and \sum_a), of the ZnO wurtzite-hexagonal structure. The dominant diffraction peak, i.e., (002), has been selected to calculate these structural properties for different RF plasma powers. The lattice constants (*a* and *c*) of ZnO are determined from the following equations⁴³

$$a = \sqrt{\frac{1}{3}} \frac{\lambda}{\sin \theta} \quad (1)$$

$$c = \frac{\lambda}{\sin \theta} \quad (2)$$

where λ is the wavelength of the X-ray source, 1.5418 Å, and θ is the angle of the diffraction peak.

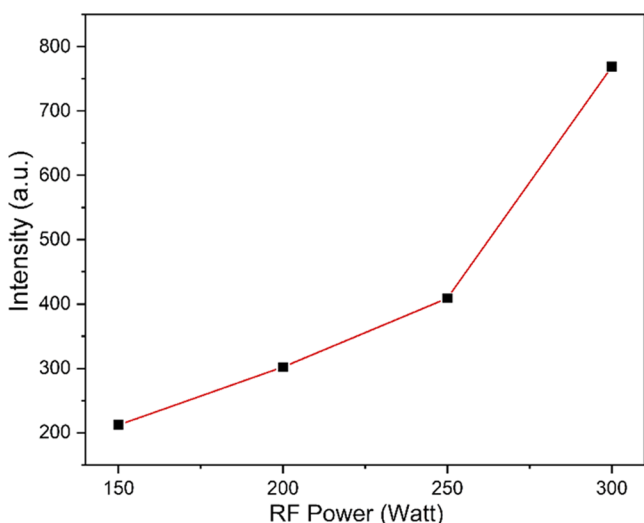


Figure 6. Impact of the RF plasma power on the (002) plane intensity for the ZnO nanostructure.

The aspect ratios (length/diameter of the ZnO nanostructure) with different RF plasma powers are shown in Table 1. It can be noticed that the aspect ratios are constant, ~ 1.732 , i.e., the RF plasma power does not impact the aspect ratio values. Reeber computed the lattice constants of the ZnO wurtzite structure at room temperature, values of c and a being 5.2075 and 3.25 Å, respectively, and the resultant c/a ratio was 1.633.⁴⁴ Unlike the RF plasma power, Karnati et al. showed that the pulsed laser deposition (PLD) technique has a remarkable impact on the aspect ratio deviation.²⁶ They have shown that the corresponding aspect ratio for 5000, 10 000, and 15 000 shots is 1.56, 1.59, and 1.65, respectively. The high aspect ratio is a result of the high surface-to-volume ratio of the ZnO nanostructure.⁴⁵ Therefore, the high surface area-to-volume ratio of the ZnO nanostructure boosts the electron-hole pair recombination, which results in a quicker decay time.⁴⁶

The strains (\sum_a and \sum_c) of ZnO along the a -axis and the c -axis, respectively, are estimated from the following equations⁴⁷

$$\sum_a = \frac{a - a_0}{a_0} \times 100\% \quad (3)$$

$$\sum_c = \frac{c - c_0}{c_0} \times 100\% \quad (4)$$

where a_0 and c_0 represent the typical lattice constants for unstrained ZnO structures that can be found from the database.⁴⁸

The observed negative value of both (\sum_a) and (\sum_c) is concerned with the compressive strain, while the positive values of strain are related to an expansion in lattice constant.

Also, the interplanar distance of ZnO is determined using Bragg's law,⁴⁹ and its results are summarized in Table 1

$$\frac{1}{d^2} = \frac{4}{3} \left(\frac{h^2 + hk + k^2}{a^2} \right) + \frac{l^2}{c^2} \quad (5)$$

where a and c are the lattice constants.

The average crystal size (D) of the fabricated ZnO nanostructure at different RF plasma powers is evaluated using Scherrer's equation as shown in Figure 7⁴⁹

$$D = \frac{k\lambda}{\beta \cos \theta} \quad (6)$$

where k is a constant equal to 0.9, λ is the wavelength of the X-ray source, β is the full width at half-maximum (FWHM), and θ is the center of the diffraction peak.

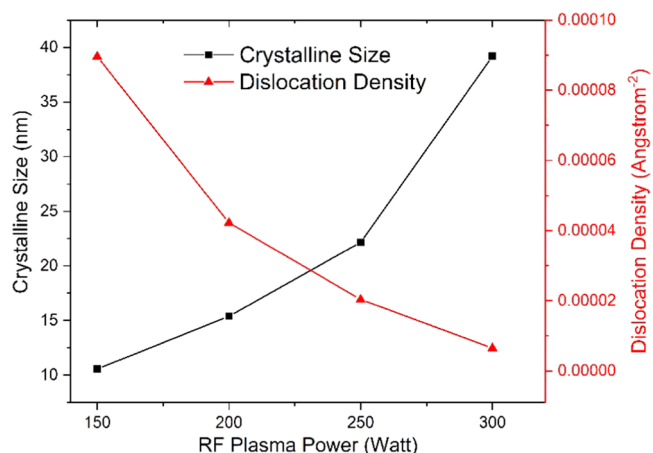


Figure 7. RF plasma power versus crystalline size and the dislocation density of the ZnO nanostructure along diffraction peak (002).

From Figure 7, it can be noted that the average crystal size increased from 10 to 40 nm as the RF plasma power increased. These noticeable increases in the crystalline size values are, perhaps, due to two main reasons. First, a high RF plasma power leads to the ZnO particle merging activity. Second, increasing the RF plasma power from 150 to 300 W leads to a decrease in FWHM values from 0.7872 to 0.2122 along the (002) plane, and therefore this peak becomes higher and narrower at the same time as shown in Table 1. Additionally, the dislocation density (δ) represents the defects in the crystal growth due to the lattice mismatch between substrate and nanostructure deposition and impurities. The (δ) value is inversely proportional to the square of the crystal size displayed in Figure 7⁵⁰

$$\delta = \frac{1}{D^2} \quad (7)$$

Table 1. Structural Properties and Lattice Constants of the ZnO Nanostructure along the Diffraction Peak (002) for Different RF Plasma Powers

RF plasma power (W)	FWHM	a (Å)	c (Å)	c/a	\sum_a %	\sum_c %	d (Å)
150	0.7872	3.00580	5.206	1.732	-7.613	-0.170	2.6031
200	0.5403	3.00707	5.208	1.732	-7.574	-0.128	2.6042
250	0.3754	3.00867	5.211	1.732	-7.522	-0.072	2.6056
300	0.2122	3.00962	5.213	1.732	-7.496	-0.044	2.6064

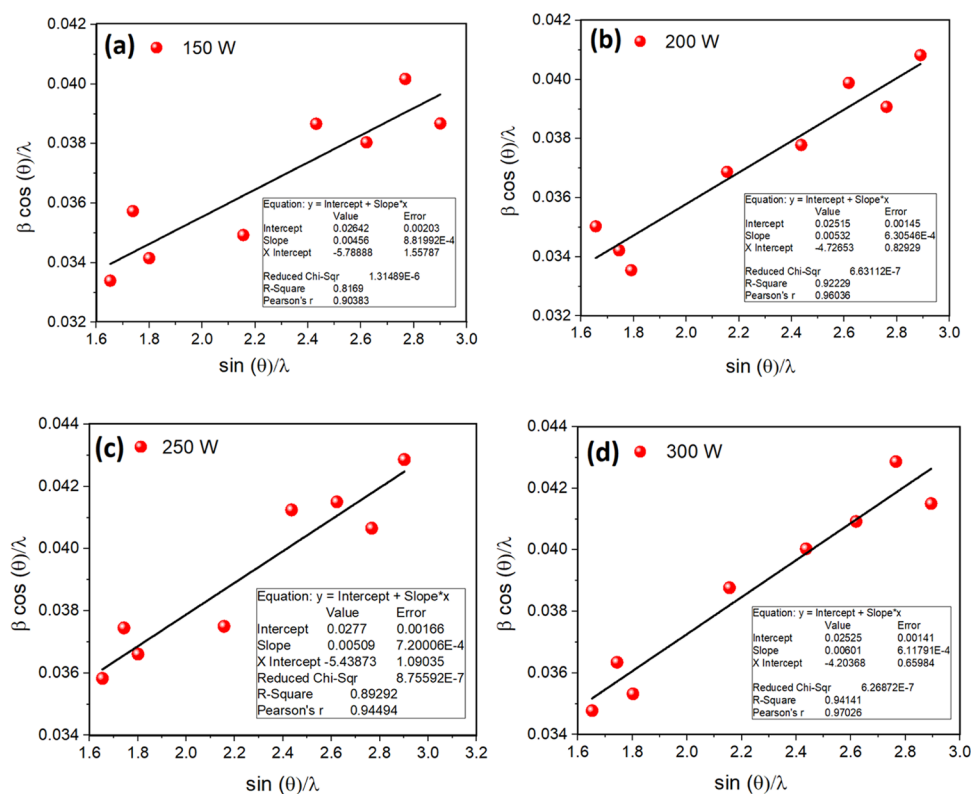


Figure 8. Williamson–Hall plot of ZnO nanorods prepared with different RF plasma powers: (a) 150 W, (b) 200 W, (c) 250 W, and (d) 300 W.

Even though the Debye Scherrer method is a well-known method that utilizes X-ray diffraction to obtain the crystalline size using FWHM of the diffraction peaks, it does not take into consideration peak broadening, which is a result of the nonhomogeneous strain and instrumental impacts. Accordingly, to obtain further information about the crystalline size of the investigated ZnO nanostructures, it is recommended to utilize the Williamson–Hall plot, which provides information regarding the lattice strain and the actual particle size and particle size with a null strain of the sample. The Williamson–Hall⁵¹ equation is expressed as

$$\frac{\beta \cos \theta}{\lambda} = \frac{1}{D_{\text{actual}}} + \frac{\mu \sin \theta}{\lambda} \quad (8)$$

where D_{actual} and μ are the actual particle size and the actual strain, respectively. Figure 8 shows the relationship between $(\beta \cos \theta)/\lambda$ against $(\sin \theta)/\lambda$, i.e., the Williamson–Hall plot. It can be noticed, from Figure 8, that the slope of the acquired linear relationship is positive, which can originate from the likelihood of tensile strain in the examined ZnO nanostructures.⁵² The computed value of the tensile strain, the slope of the graph, for different RF plasma powers, 150, 200, 250, and 300 W, was found to be 0.38, 0.33, 0.31, and 0.28%, respectively, while the effective particle size values for different RF plasma powers, 150, 200, 250, and 300 W, were calculated to be 15, 20, 35, and 47 nm, respectively. It can be stated that the value of the crystalline size computed using the Scherrer equation is smaller than that acquired through the Williamson–Hall method. This alteration is ascribed to the strain value and illustrates that the role of strain is significant; thus, it should be considered in the measurement of the crystalline size. Therefore, utilizing the Scherrer equation, which does not consider the strain, might produce imprecise

outcomes. The lattice strain shown by the Williamson–Hall plot displayed a reduction with an increase in the RF plasma power. The growth mechanism in general causes some strains in the crystal.⁵³ Once the RF plasma power was amplified, the domain structure was overdrawn and released the additional strain, and in this manner, a crystalline size decrease was acquired by increasing the RF plasma power.

3.5. Optical Property Analysis. Figure 9 shows the UV–vis transmittance spectrum for the synthesized ZnO nanostructure at different plasma powers from 150 to 300 W. All of the ZnO samples possess low transmittance in the UV region,

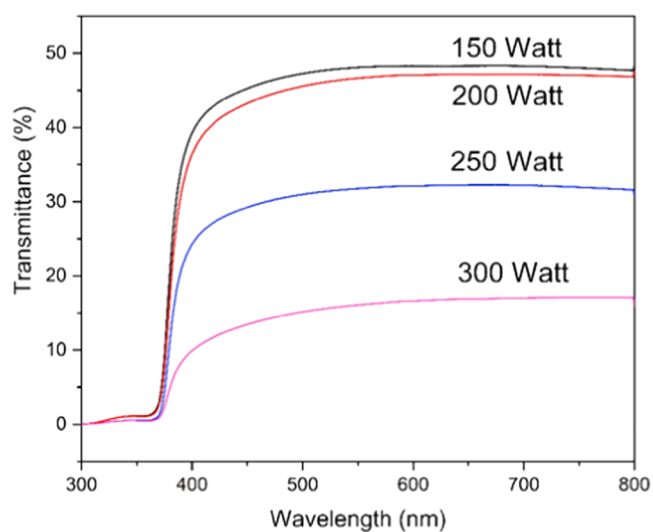


Figure 9. Optical transmittance spectrum of the ZnO nanostructure synthesized at different RF plasma powers.

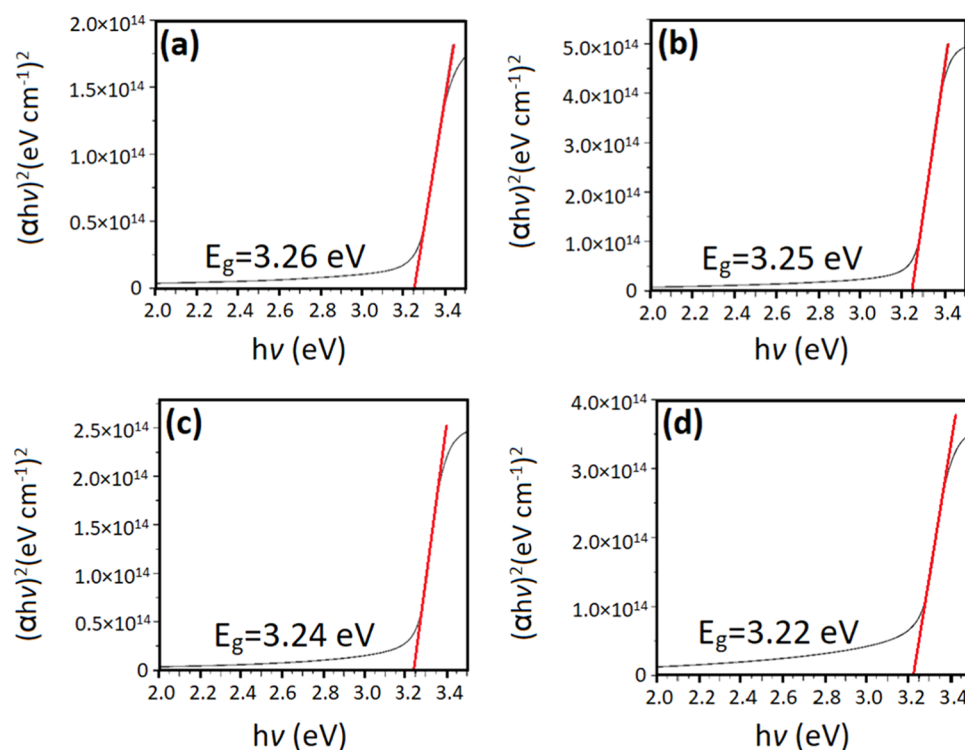


Figure 10. Energy band-gap measurement for the ZnO nanostructure using different RF plasma powers: (a) 150 W, (b) 200 W, (c) 250 W, and (d) 300 W.

$\lambda < 400$ nm, and high transmittance in the visible region, $\lambda > 400$. It was observed that the highest transmittance corresponded to 150 W; then, it decreased from ~ 48 to $\sim 17\%$ as the plasma power was increased up to 300 W. This is possibly due to the increase of the scattering light from oxygen vacancies, Zn interstitials, dislocation density, and the nanostructure thickness.^{54,55} Moreover, once the RF plasma power increases, the transmittance spectrum shifts to the longer wavelength.⁵⁶ This is more likely due to the internal stress produced inside the nanorods and the light-scattering effects as a result of surface roughness. Chatterjee et al.⁵⁷ have shown that argon ion bombardment produces a nanoscale roughening of the nanorod sidewalls. This nanoscale roughening possesses a wide range of applications, such as in catalysis, gas sensing, solar cells, field emission, and gas discharge. Also, ion bombardment leads to an increase in the oxygen vacancies near the surface and hence a change in the electrical properties.⁵⁸ In addition, increasing the RF power leads to an increase of the ZnO thickness.⁵⁹

The optical band-gap energy (E_g) of the ZnO nanostructure prepared at different RF plasma powers can be calculated using Tauc's relation as shown in Figure 10.⁶⁰

$$(\alpha h\nu)^2 = A(h\nu - E_g)^n \quad (9)$$

where α is the absorption coefficient, $h\nu$ is the photon energy, A is a constant, E_g is the optical band gap energy, and n depends on the type of transmission ($n = 1/2$ due to the direct transmission of ZnO). For the transmittance spectrum, the α coefficient can be calculated using⁶¹

$$\alpha = \frac{\ln\left(\frac{1}{T}\right)}{d} \quad (10)$$

where T is the transmittance of the ZnO samples and d is the thickness of ZnO.

From the plots, it was observed that the transition region is at around 3.20 eV, which corresponds to the direct band-gap energy (E_g) of the ZnO semiconductor.⁴ The optical band gap decreases from 3.26 to 3.22 eV on increasing the RF plasma power from 150 to 300 W, respectively. These values are lower than the value of bulk ZnO, which is 3.4 eV.⁶² The obtained values of E_g in this study are in good agreement with the values (3.25–3.32 eV) reported by Ma et al. for ZnO prepared at a low plasma power.⁶³ In a similar study by El-Hossary et al.,²⁴ it was shown that the optical band gap decreases from 3.35 to 3.05 eV on increasing the RF power from 300 to 500 W, respectively. In fact, the quantum size effect and the Burstein–Moss effect together increase the optical band gap, whereas lower oxygen contents and higher defects reduce the band gap.²⁴

It is worth noting that the E_g value is correlated to several factors, such as the dislocation density, defects (oxygen vacancies, Zn interstitials), strain, random orientation of nanorods, and the quantum size effect of the nanostructure, which have already been proved by the XRD results.^{64,65}

On the other hand, the increasing band gap is owing to the existence of zinc hydroxide, Zn(OH)₂.⁶⁶ The band gap was found to decrease from 3.26 to 3.22 eV after increasing the RF plasma power from 150 to 300 W as a result of the removal of Zn(OH)₂ from the film or elimination of defect levels after increasing the RF plasma power, which is a more common phenomenon in chemically deposited thin films.⁶⁷ Wang et al.⁶⁸ stated that the optical energy band-gap broadening can be achieved through Al-doped ZnO thin films. Elimination of piling faults results in the orientation of separate crystallites and the existence of defect-free grain boundaries. Jimenez-Gonzalez and Nair⁶⁹ described the reduction in the band gap

after increasing the temperature of ZnO thin films as due to the quantum confinement of the charge carriers in extrinsic nanocrystalline grains. Paul et al.⁴² showed that noticeable green emission in the photoluminescence spectrum, predominantly related to the oxygen vacancies on the surface of the ZnO nanostructure, is considerably eliminated by the amalgamation of glucose biomolecules. Reaz et al.⁷⁰ show the effective synthesis and adoption of ZnO/iron oxide core-shell nanoparticles with variable magnetic characteristics. They confirmed that structural alterations at the nanolevel, after determining adjustments between the core-shell nanoparticle samples, have an important influence on their magnetic and fluorescent properties. In another attempt, Mohamed et al.⁷¹ investigated the impacts of consecutive plasma processing cyclic times on the structure, optical properties, and electrical resistivity of ZnO thin films. They showed that the grain size can be reduced to some extent as the treatment time increases, while the optical band gap increases on increasing the plasma treatment time.

4. CONCLUSIONS

ZnO nanostructural thin films are successfully synthesized on glass substrates using the radio frequency sputtering magnetron technique without any foreign catalyst. In this study, the impact of the variation of plasma power on the morphology, structure, crystalline size, dislocation density, and energy band gap of the ZnO nanostructure has been investigated. This study shows that the stoichiometry in the Zn/O ratio is also affected by variation of the RF plasma power. SEM and XRD analyses indicated that the RF plasma power has a clear impact on the shape and the size of the ZnO nanostructure and a preferential growth direction along (002) orientation is dominant. In addition, the average diameter of the ZnO nanostructure is changed gradually in the range of 14–202 nm as the RF plasma power increases from 150 to 300 W. Moreover, the crystal qualities of the ZnO nanostructure improved, as displayed by the sharpening and the narrowing of the X-ray diffraction peaks, on the polar surface *c*-axis with a reduction in the dislocation density at higher plasma powers. The highest optical transmittance spectrum from the ZnO nanostructure is observed at 150 W of plasma power; however, it decreases dramatically from ~48 to ~17% as the plasma power increases from 150 to 300 W. This is possibly due to the increase in the scattering light from voids, grain size, and the thickness of the ZnO nanostructure. The UV-vis absorption spectrum indicates that the energy band gap slightly decreases from 3.26 to 3.22 eV with an increasing RF plasma power, as a result of defects, strains, thickness, and random orientation of the ZnO nanostructure.

AUTHOR INFORMATION

Corresponding Author

Azeez A. Barzinjy – Department of Physics, College of Education, Salahaddin University-Erbil, Erbil 44001 Kurdistan Region, Iraq; Department of Physics Education, Faculty of Education, Tishk International University, Erbil 44001 Kurdistan Region, Iraq; orcid.org/0000-0003-4009-9845; Phone: 009647504542010; Email: azeez.azeez@su.edu.krd

Authors

Ahmed F. Abdulrahman – Department of Physics, Faculty of Science, University of Zakho, Zakho 42002 Kurdistan Region, Iraq

Samir M. Hamad – Scientific Research Centre, Soran University, Soran-Erbil 44008 Kurdistan Region, Iraq

Munirah Abdullah Almessiere – Department of Physics, College of Science and Department of Biophysics, Institute for Research and Medical Consultation (IRMC), Imam Abdulrahman Bin Faisal University, 31441 Dammam, Saudi Arabia; orcid.org/0000-0003-1651-3591

Complete contact information is available at:
<https://pubs.acs.org/10.1021/acsoomega.1c04105>

Notes

The authors declare no competing financial interest.

REFERENCES

- (1) Diao, F.; Wang, Y. Transition metal oxide nanostructures: premeditated fabrication and applications in electronic and photonic devices. *J. Mater. Sci.* **2018**, *53*, 4334–4359.
- (2) Leung, S.-F.; Zhang, Q.; Xiu, F.; Yu, D.; Ho, J. C.; Li, D.; Fan, Z. Light management with nanostructures for optoelectronic devices. *J. Phys. Chem. Lett.* **2014**, *5*, 1479–1495.
- (3) Kolodziejczak-Radzimska, A.; Jesionowski, T. Zinc oxide—from synthesis to application: a review. *Materials* **2014**, *7*, 2833–2881.
- (4) Abdulrahman, A. F.; Ahmed, S. M.; Almessiere, M. A. EFFECT OF THE GROWTH TIME ON THE OPTICAL PROPERTIES OF ZnO NANORODS GROWN BY LOW TEMPERATURE METHOD. *Dig. J. Nanomater. Biostruct.* **2017**, *12*, 1001–1009.
- (5) Ghorai, A.; Bayan, S.; Gogurla, N.; Midya, A.; Ray, S. K. Highly luminescent WS₂ quantum dots/ZnO heterojunctions for light emitting devices. *ACS Appl. Mater. Interfaces* **2017**, *9*, 558–565.
- (6) Lupan, O.; Postica, V.; Pauporte, T.; Viana, B.; Terasa, M.-I.; Adelung, R. Room temperature gas nanosensors based on individual and multiple networked Au-modified ZnO nanowires. *Sens. Actuators, B* **2019**, *299*, No. 126977.
- (7) Wu, D.; Wang, Y.; Ma, N.; Cao, K.; Zhang, W.; Chen, J.; Wang, D.; Gao, Z.; Xu, F.; Jiang, K. Single-crystal-like ZnO mesoporous spheres derived from metal organic framework delivering high electron mobility for enhanced energy conversion and storage performances. *Electrochim. Acta* **2019**, *305*, 474–483.
- (8) Das, D.; Karmakar, L. Optimization of Si doping in ZnO thin films and fabrication of n-ZnO: Si/p-Si heterojunction solar cells. *J. Alloys Compd.* **2020**, *824*, No. 153902.
- (9) Barzinjy, A. A.; Hamad, S. M.; Esmaeel, M. M.; Aydın, S. K.; Hussain, F. H. S. Biosynthesis and characterisation of zinc oxide nanoparticles from Punica granatum (pomegranate) juice extract and its application in thin films preparation by spin-coating method. *Micro Nano Lett.* **2020**, *15*, 415–420.
- (10) George, A.; Kumari, P.; Soin, N.; Roy, S.; McLaughlin, J. Microstructure and field emission characteristics of ZnO nanoneedles grown by physical vapor deposition. *Mater. Chem. Phys.* **2010**, *123*, 634–638.
- (11) Chatterjee, S.; Gohil, S.; Chalke, B.; Ayyub, P. Optimization of the morphology of ZnO nanorods grown by an electrochemical process. *J. Nanosci. Nanotechnol.* **2009**, *9*, 4792–4796.
- (12) Ponja, S. D.; Sathasivam, S.; Parkin, I. P.; Carmalt, C. J. Highly conductive and transparent gallium doped zinc oxide thin films via chemical vapor deposition. *Sci. Rep.* **2020**, *10*, No. 638.
- (13) von Wenckstern, H.; Splith, D.; Grundmann, M. Pulsed Laser Deposition 2 of Ga₂O₃ and Related Alloys. In *Gallium Oxide: Materials Properties, Crystal Growth, and Devices*; Springer: Cham, 2020; pp 273–291.
- (14) Ganesan, V.; Hariram, M.; Vivekanandhan, S.; Muthuramkumar, S. Periconium sp.(endophytic fungi) extract mediated sol-gel synthesis of ZnO nanoparticles for antimicrobial

and antioxidant applications. *Mater. Sci. Semicond. Process.* **2020**, *105*, No. 104739.

(15) Saha, J. K.; Billah, M. M.; Bukke, R. N.; Kim, Y. G.; Mude, N. N.; Siddik, A. B.; Islam, M. M.; Do, Y.; Choi, M.; Jang, J. Highly Stable, Nanocrystalline, ZnO Thin-Film Transistor by Spray Pyrolysis Using High-K Dielectric. *IEEE Trans. Electron Devices* **2020**, *67*, 1021–1026.

(16) Sun, L.; Shao, Q.; Zhang, Y.; Jiang, H.; Ge, S.; Lou, S.; Lin, J.; Zhang, J.; Wu, S.; Dong, M.; et al. N self-doped ZnO derived from microwave hydrothermal synthesized zeolitic imidazolate framework-8 toward enhanced photocatalytic degradation of methylene blue. *J. Colloid Interface Sci.* **2020**, *565*, 142–155.

(17) Stamate, E. Lowering the resistivity of aluminum doped zinc oxide thin films by controlling the self-bias during RF magnetron sputtering. *Surf. Coat. Technol.* **2020**, *402*, No. 126306.

(18) Tang, P.; Li, B.; Feng, L. The optical and electrical properties of ZnO: Al thin films deposited at low temperatures by RF magnetron sputtering. *Ceram. Int.* **2018**, *44*, 4154–4157.

(19) Kumeta, K.; Ono, H.; Iizuka, S. Formation of ZnO nanostructures in energy-controlled hollow-type magnetron RF plasma. *Thin Solid Films* **2010**, *518*, 3522–3525.

(20) Xu, S.; Long, J.; Sim, L.; Diong, C. H.; Ostrikov, K. RF plasma sputtering deposition of hydroxyapatite bioceramics: synthesis, performance, and biocompatibility. *Plasma Processes Polym.* **2005**, *2*, 373–390.

(21) Kuo, S.-Y.; Liu, K.-C.; Lai, F.-L.; Yang, J.-F.; Chen, W.-C.; Hsieh, M.-Y.; Lin, H.-I.; Lin, W.-T. Effects of RF power on the structural, optical and electrical properties of Al-doped zinc oxide films. *Microelectron. Reliab.* **2010**, *50*, 730–733.

(22) Borchard, P. Electron beam gun with kinematic coupling for high power RF vacuum devices. US 9,502,203 B1, 2016.

(23) Lee, H.-C.; Seo, B.; Kwon, D.-C.; Kim, J.; Seong, D.; Oh, S.; Chung, C.-W.; You, K.; Shin, C. Evolution of electron temperature in inductively coupled plasma. *Appl. Phys. Lett.* **2017**, *110*, No. 014106.

(24) El-Hossary, F.; Mohamed, S.; Noureldein, E.; EL-Kassem, M. A. Influence of rf power on growth, structural and optical properties of ZnO synthesized via vapor transport in inductively coupled plasma. *Mater. Sci. Semicond. Process.* **2020**, *120*, No. 105284.

(25) Irzh, A.; Genish, I.; Klein, L.; Solovyov, L. A.; Gedanken, A. Synthesis of ZnO and Zn nanoparticles in microwave plasma and their deposition on glass slides. *Langmuir* **2010**, *26*, 5976–5984.

(26) Karnati, P.; Haque, A.; Taufique, M.; Ghosh, K. A systematic study on the structural and optical properties of vertically aligned zinc oxide nanorods grown by high pressure assisted pulsed laser deposition technique. *Nanomaterials* **2018**, *8*, No. 62.

(27) Fan, H. J.; Werner, P.; Zacharias, M. Semiconductor nanowires: from self-organization to patterned growth. *Small* **2006**, *2*, 700–717.

(28) Otieno, F.; Airo, M.; Ganetsos, T.; Erasmus, R. M.; Billing, D. G.; Quandt, A.; Wamwangi, D. Role of oxygen concentrations on structural and optical properties of RF magnetron sputtered ZnO thin films. *Opt. Quantum Electron.* **2019**, *51*, No. 359.

(29) Martín-Palma, R. J.; Lakhtakia, A. Chapter 15-Vapor-Deposition Techniques. In *Engineered Biomimicry*; Elsevier Inc., 2013; pp 383–398.

(30) Cullen, P.; Milosavljević, V. Spectroscopic characterization of a radio-frequency argon plasma jet discharge in ambient air. *Prog. Theor. Exp. Phys.* **2015**, *2015*, No. 63J01.

(31) Vallée, C.; Bonvalot, M.; Belahcen, S.; Yeghoyan, T.; Jaffal, M.; Vallat, R.; Chaker, A.; Lefèvre, G.; David, S.; Bsiesy, A. Plasma deposition—Impact of ions in plasma enhanced chemical vapor deposition, plasma enhanced atomic layer deposition, and applications to area selective deposition. *J. Vac. Sci. Technol., A* **2020**, *38*, No. 033007.

(32) Dai, H.; Yu, X.; Zhao, Z.; Shi, D.; Shi, X.; Zhao, J.; Dong, X.; Zhang, D. Low Temperature RF-Plasma Initiated Rapid and Highly Ordered Fracture on Ag Nanowires. *Appl. Sci.* **2020**, *10*, No. 1338.

(33) Zhou, R.; Zhou, R.; Wang, P.; Xian, Y.; Mai-Prochnow, A.; Lu, X.; Cullen, P.; Ostrikov, K. K.; Bazaka, K. Plasma-activated water:

generation, origin of reactive species and biological applications. *J. Phys. D: Appl. Phys.* **2020**, *53*, No. 303001.

(34) Kwon, J. H.; Kim, D. Y.; Kim, K.-S.; Hwang, N.-M. Preparation of highly (002) oriented Ti films on a floating Si (100) substrate by RF magnetron sputtering. *Electron. Mater. Lett.* **2020**, *16*, 14–21.

(35) Li, C.; Wang, D.; Li, Z.; Li, X.; Kawaharamura, T.; Furuta, M. Stoichiometry control of ZnO thin film by adjusting working gas ratio during radio frequency magnetron sputtering. *J. Mater.* **2013**, *2013*, 1–6.

(36) Hu, Y.; L F, W.; Xu, H.; Chen, Y.; Jiang, W. In *The Low-Cost Preparation of Pyramid-like Texture ZnO Thin Films and the Application as a Front Electrode in Hydrogen Amorphous Silicon Solar Cells*, 5th International Symposium on Advanced Optical Manufacturing and Testing Technologies: Optoelectronic Materials and Devices for Detector, Imager, Display, and Energy Conversion Technology; International Society for Optics and Photonics, 2010; p 76580D.

(37) Spadoni, A.; Addonizio, M. Effect of the RF sputtering power on microstructural, optical and electrical properties of Al doped ZnO thin films. *Thin Solid Films* **2015**, *589*, 514–520.

(38) Srinatha, N.; No, Y.; Kamble, V. B.; Chakravarty, S.; Suriyamurthy, N.; Angadi, B.; Umarji, A.; Choi, W. Effect of RF power on the structural, optical and gas sensing properties of RF-sputtered Al doped ZnO thin films. *RSC Adv.* **2016**, *6*, 9779–9788.

(39) Hu, Y.-H.; Yi-Chuan, C.; Hai-Jun, X.; Hao, G.; Wei-Hui, J.; Fei, H.; Yan-Xiang, W. Texture ZnO thin-films and their application as front electrode in solar cells. *Engineering* **2010**, *2*, 973–978.

(40) Jagadale, S. B.; Patil, V. L.; Vanalakar, S. A.; Patil, P. S.; Deshmukh, H. P. Preparation, characterization of 1D ZnO nanorods and their gas sensing properties. *Ceram. Int.* **2018**, *44*, 3333–3340.

(41) Bhaumik, A.; Haque, A.; Karnati, P.; Taufique, M.; Patel, R.; Ghosh, K. Copper oxide based nanostructures for improved solar cell efficiency. *Thin Solid Films* **2014**, *572*, 126–133.

(42) Paul, B.; Abdullah-Al Mamun, M.; Haque, A.; Paul, M.; Ghosh, K. Significant reduction of defect states and surface tailoring in ZnO nanoparticles via nano-bio interaction with glucose for bio-applications. *IEEE Trans. Nanobiosci.* **2019**, *18*, 490–497.

(43) Abdulrahman, A. F.; Ahmed, S. M.; Ahmed, N. M. Investigation of optical properties of ZnO nanorods grown on different substrates. *Sci. J. Univ. Zakho* **2018**, *6*, 160–165.

(44) Reeber, R. R. Lattice parameters of ZnO from 4.2 to 296 K. *J. Appl. Phys.* **1970**, *41*, 5063–5066.

(45) Ahmed, F.; Arshi, N.; Anwar, M.; Danish, R.; Koo, B. H. Morphological evolution of ZnO nanostructures and their aspect ratio-induced enhancement in photocatalytic properties. *RSC Adv.* **2014**, *4*, 29249–29263.

(46) Vabbina, P. K.; Kaushik, A.; Pokhrel, N.; Bhansali, S.; Pala, N. Electrochemical cortisol immunosensors based on sonochemically synthesized zinc oxide 1D nanorods and 2D nanoflakes. *Biosens. Bioelectron.* **2015**, *63*, 124–130.

(47) Abdulrahman, A. F. The effect of different substrate-inclined angles on the characteristic properties of ZnO nanorods for UV photodetectors applications. *J. Mater. Sci.: Mater. Electron.* **2020**, *31*, 14357–14374.

(48) Abdulrahman, A. F.; Ahmed, S. M.; Barzinjy, A. A.; Hamad, S. M.; Ahmed, N. M.; Almessiere, M. A. Fabrication and Characterization of High-Quality UV Photodetectors Based ZnO Nanorods Using Traditional and Modified Chemical Bath Deposition Methods. *Nanomaterials* **2021**, *11*, No. 677.

(49) Abdulrahman, A. F.; Ahmed, S. M.; Ahmed, N. M.; Almessiere, M. A. Enhancement of ZnO nanorods properties using modified chemical bath deposition method: effect of precursor concentration. *Crystals* **2020**, *10*, No. 386.

(50) Abdulrahman, A. F. Study the optical properties of the various deposition solutions of ZnO nanorods grown on glass substrate using chemical bath deposition technique. *J. Ovonic Res.* **2020**, *16*, 181–188.

(51) Williamson, G.; Hall, W. X-ray line broadening from filed aluminium and wolfram. *Acta Metall.* **1953**, *1*, 22–31.

(52) Senthilkumar, V.; Vickraman, P.; Jayachandran, M.; Sanjeeviraja, C. Structural and electrical studies of nano structured

- Sn $1-x$ Sb x O 2 ($x= 0.0, 1, 2.5, 4.5$ and 7 at%) prepared by co-precipitation method. *J. Mater. Sci.: Mater. Electron.* **2010**, *21*, 343–348.
- (53) Zhao, J.; Jin, Z.-G.; Liu, X.-X.; Liu, Z.-F. Growth and morphology of ZnO nanorods prepared from Zn (NO₃)₂/NaOH solutions. *J. Eur. Ceram. Soc.* **2006**, *26*, 3745–3752.
- (54) Singh, P.; Kumar, A.; Kaur, D.; et al. Growth and characterization of ZnO nanocrystalline thin films and nanopowder via low-cost ultrasonic spray pyrolysis. *J. Cryst. Growth* **2007**, *306*, 303–310.
- (55) Kaphle, A.; Hari, P. Enhancement in power conversion efficiency of silicon solar cells with cobalt doped ZnO nanoparticle thin film layers. *Thin Solid Films* **2018**, *657*, 76–87.
- (56) Fernández, S.; Naranjo, F. Optimization of aluminum-doped zinc oxide films deposited at low temperature by radio-frequency sputtering on flexible substrates for solar cell applications. *Sol. Energy Mater. Sol. Cells* **2010**, *94*, 157–163.
- (57) Chatterjee, S.; Behera, A. K.; Banerjee, A.; Tribedi, L. C.; Som, T.; Ayyub, P. Nanometer-scale sharpening and surface roughening of ZnO nanorods by argon ion bombardment. *Appl. Surf. Sci.* **2012**, *258*, 7016–7020.
- (58) Ra, H.-W.; Choi, K.; Ok, C.; Jo, S.; Bai, K.; Im, Y. Ion bombardment effects on ZnO nanowires during plasma treatment. *Appl. Phys. Lett.* **2008**, *93*, No. 033112.
- (59) Yang, K.; Li, B.; Zeng, G. Effects of temperature on properties of ZnS thin films deposited by pulsed laser deposition. *Superlattices Microstruct.* **2019**, *130*, 409–415.
- (60) Qasim, A. K.; Jamil, L. A.; Abdulrahman, A. F. Synthesis of Rutile-TiO₂ Nanorod Arrays for Efficient Solar Water Splitting Via Microwave-Assisted Hydrothermal Method. *Dig. J. Nanomater. Biostruct.* **2020**, *15*, 157–165.
- (61) Akhiruddin, A.; Sugianto, S.; Irmansyah, I. The influence of hydrothermal duration on structures and optical properties of ZnO nanoparticles. *J. Mater. Phys. Chem.* **2015**, *2*, 34–37.
- (62) Barzinjy, A. A.; Azeez, H. H. Green synthesis and characterization of zinc oxide nanoparticles using *Eucalyptus globulus* Labill. leaf extract and zinc nitrate hexahydrate salt. *SN Appl. Sci.* **2020**, *2*, No. 991.
- (63) Ma, A.; Rousseau, F.; Donsanti, F.; Lincot, D.; Morvan, D. Deposition of ZnO thin films from aqueous solution in a low power plasma reactor. *Surf. Coat. Technol.* **2015**, *276*, 186–194.
- (64) Singh, N. K.; Rajkumari, R. Chapter 7-Effect of Annealing on Metal-Oxide Nanocluster. In *Concepts of Semiconductor Photocatalysis*; IntechOpen, 2019; pp 121–134.
- (65) Asgary, S.; Ramezani, A. H.; Mahmoodi, A. Physical properties of nanostructured ZnO thin films deposited by dc magnetron sputtering method with different volume of O₂ in a carrier gas. *J. Min. Metall., Sect. B* **2019**, *55*, 111–120.
- (66) Olvera, M. D. L. L.; Maldonado, A.; Asomoza, R.; Melendez-Lira, M. Effect of the substrate temperature and acidity of the spray solution on the physical properties of F-doped ZnO thin films deposited by chemical spray. *Sol. Energy Mater. Sol. Cells* **2002**, *71*, 61–71.
- (67) Hodes, G.; Albu-Yaron, A.; Decker, F.; Motisuke, P. Three-dimensional quantum-size effect in chemically deposited cadmium selenide films. *Phys. Rev. B* **1987**, *36*, No. 4215.
- (68) Wang, F.-H.; Chang, H.-P.; Tseng, C.-C.; Huang, C.-C. Effects of H₂ plasma treatment on properties of ZnO: Al thin films prepared by RF magnetron sputtering. *Surf. Coat. Technol.* **2011**, *205*, 5269–5277.
- (69) Jimenez-Gonzalez, A.; Nair, P. Photosensitive ZnO thin films prepared by the chemical deposition method SILAR. *Semicond. Sci. Technol.* **1995**, *10*, 1277.
- (70) Reaz, M.; Haque, A.; Cornelison, D.; Wanekaya, A.; Delong, R.; Ghosh, K. Magneto-luminescent zinc/iron oxide core-shell nanoparticles with tunable magnetic properties. *Phys. E* **2020**, *123*, No. 114090.
- (71) Mohamed, S.; Abd El-Rahman, A.; Salem, A.; Pichon, L.; El-Hossary, F. Effect of rf plasma nitriding time on electrical and optical properties of ZnO thin films. *J. Phys. Chem. Solids* **2006**, *67*, 2351–2357.